Egypt. J. Chem. **Vol.** 64, No. 10 pp. 6123 - 6135 (2021)

Egyptian Journal of Chemistry

http://ejchem.journals.ekb.eg/

The Performance of Inorganic Salts/PMMA Nanocomposites in Ca^{+2} and Mg^{+2} Adsorption from Aqueous Solution

Sanaa M. Solyman[1], Hager R. Ali[2*], Yasser M. Moustafa[2]

[1] *Petrochemical department, Egyptian petroleum research institute, Nasr City, PO Box 11727, Cairo, Egypt.*

[2] *Analysis and Evaluation department, Central lab. Egyptian petroleum research institute, Nasr City, PO Box 11727, Cairo, Egypt.*

**Corresponding author E-mail: hagerchem@gmail.com*

Abstract

This study aimed to synthesize a new hybrid polymethyl methacrylate (PMMA) nanocomposite as catalysts in water treatment with high efficiency. We prepared three different materials, PMMA alone, then $TiSO_4$/PMMA, and $CaSO_4$/PMMA. After that, we made a screening experiment and found that $TiSO_4$/PMMA was effective for Ca^{+2} removal and $CaSO_4$/PMMA was effective for Mg^{+2} removal, and we made the optimization process according to this principle. The pH, contact time, dose, initial pollutant concentration, and temperature were performed to obtain the optimum parameters that achieve the highest Ca^{+2}, Mg^{+2} removal efficiency as main cations causing hardness. The nanocomposite samples were characterized using different techniques. The $CaSO_4$ nanoparticles were distributed uniformly across the $CaSO_4$/PMMA matrix but $TiSO_4$/PMMA has the parallel plate's morphology. Accordingly, the structures of the hybrids have been postulated. The maximum elimination value was 87.5% for Ca^{+2} and 65% for Mg^{+2}. Adsorption isotherm and kinetics were demonstrated to set the nature of the reaction. Langmuir adsorption isotherm models were fitted with the experimental data for Mg^{+2} and Ca^{+2}. The data of the pseudo-second-order kinetic model adequately fit the experimental values for the adsorption of Mg^{+2} and Ca^{+2}. The positive values of ΔG^o for Ca^{+2} (1.86 to 5.8 KJ/mol) at all temperatures, and ΔG^o for Mg^{+2} (1.5 KJ/mol) at 25^{o}C indicated spontaneous adsorption process while the negative values for Mg^{+2} at 40^{o}C and 60^{o}C indicated a non-spontaneous adsorption process.

Keywords: Nanocomposites; Inorganic/PMMA; Postulated Structure; Ca and Mg Cations Removal; Kinetics.

1. Introduction

In addition to hydrogeochemical conditions in the aquifer that is likely to dissolve calcium (Ca^{2+}) and magnesium (Mg^{2+}), high groundwater misuse and exploitation change the hydrodynamics that leads to the development of hardness [**1, 2**]. Moreover, the industry produces saline waters that are now not suitable for use. The existence of hardness sellers discourages the usage of sea and groundwaters in the industrial and agricultural sectors or as consuming water. Hard water minerals cause troubles of scaling and enormous disasters in boiler pipes and warmth switch equipment. As a result, decreasing the salt content material is wished for most application fields. Water hardness refers to the existence of divalent ions iron, manganese, calcium, and magnesium. Calcium and magnesium are the most popular species for water hardening **[3]**. The most perfect level of hardness has now not been defined because of the fact public acceptance differs remarkably in line with nearby conditions. Water aspects with total hardness above 200 mg/L generally can be allowed via shoppers but are considered to be a bad source;

*Corresponding author e-mail: d_hager80@yahoo.com.; (Hager R. Ali).

Receive Date: 28 December 2020, Revise Date: 16 June 2021, Accept Date: 07 July 2021

DOI: 10.21608/EJCHEM.2021.55304.3172

whereas most domestic consumption values above 5 hundred mg/L are now not appropriate **[4]**. Friendly surroundings adsorbents are required to minimize the divalent cation concentration and accordingly the hardness of the water. Nanocomposites are a brand new department that may be advantageous as catalysts for the elimination of heavy metals **[5-7]** and in different fields **[8,9]**. For example, melamine grafted chitosan-montmorillonite nanocomposite for ferric ions adsorption has been studied **[7]**. The nanocomposite displays 99.97% for the removal of ferric ions with strong reusability until the third cycle under optimum conditions. Polymethyl methacrylate (PMMA) was chosen in this study because it is non-toxic, cost-effective, and effortless to get. PMMA has appropriate material properties such as distinguished mechanical quality, hardness, excessive rigidity, transparency, and good insulation residences **[10]**. Recently, some studies have been made to comprise nanoscale substances into PMMA to achieve multipurpose functional nanoparticles. The PMMA ester group can interact with metals. This interplay might also be due to physical interaction, chemical reaction, or intra-diffusion process. Previous publications studied the modulation of PMMA with the aid of Ca deposition on its surface **[10, 11]**. They concluded that Ca atoms react with the ester groups in PMMA film to form $(CH_3COO)_2Ca$ and ethane in the Ca deposition manner which indicating a chemical reaction. The deposition of noticeably reactive metals like Al, Cr, or Ni to PMMA affects robust chemical reactions resulting in some stable metal−PMMA complexes at the interface **[10]**. The modern-day learn about is the first one aimed at reading the overall performance of $TiSO_4$/PMMA and $CaSO_4$/PMMA in reducing the awareness of metallic cations. Since the Ca^{+2} and Mg^{+2} are the key cations that reason hardness, in this learn about the adsorption overall performance of these cations is a precise goal. The effect of $TiSO_4$ and $CaSO_4$ on the effectivity of PMMA purposeful groups and the morphology will be studied. PMMA nanocomposites as adsorbents provide many economic benefits and are examined for softening groundwater.

The synthesis of new hybrid polymethyl methacrylate nanocomposites as catalysts in water treatment with high efficiency is a good objective. So, PMMA and its composites $TiSO_4$/PMMA and $CaSO_4$/PMMA were prepared, characterized, and investigated in the removal of Ca^{+2} and Mg^{+2} cations as main cations causing hardness. Different factors were studied (pH, contact time, catalyst dose, initial pollutant concentration, and temperature). The screening experiments indicated that $CaSO_4$/PMMA was effective in the removal of Mg^{+2} but $TiSO_4$/PMMA was effective in the removal of Ca^{+2}. The optimum parameters that achieve the highest removal efficiency for Ca^{+2} (87.5%) and Mg^{+2} (65%) were at 40 ^oC and 25 ^oC respectively, 1g/l dose, pH 8 at 120min with constant stirring.

2. Experimental section

2.1. Materials

The chemical reagents used for nanocomposite synthesis were of industrial quality, used without purification. Methyl methacrylate (MMA), Benzoyl peroxide, Methanol (CH_3OH), Calcium chloride ($CaCl_2$), Magnesium chloride ($MgCl_2$) Polyethylene glycol (PEG) M.W=200 g/mol, Ammonium sulfate $(NH_4)_2SO_4$, and Titanium sulfate ($TiSO_4$) are bought from Sigma Aldrich company.

2.2. Hybrid nanocomposites preparation

a) Preparation of PMMA: Purified and dried 20 ml of MMA and 0.15 g of benzoyl peroxide (as initiator) were stirred at 70^{o}C for 2 hr. The PMMA was precipitated by 5% acidified methanol, washed, then dried at 80 ^{o}C overnight **[12]**.

b) Preparation of $CaSO_4$ nanoparticles was done by mixing two solutions, the first one being 11.1 g of $CaCl_2$ with a minimum amount of bidistilled water. The second solution was 24.8 g of PEG (M.W=200 g/mol) with a minimum amount of bidistilled water. The second solution of PEG was added to $CaCl_2$ (the first solution) dropwise with stirring within 15 min then continuous stirring for 4 h. This mixture was maintained at room temperature for 12 h. Then 13.2 g of $(NH_4)_2SO_4$ solution was added to the previous mixture dropwise with continuous stirring through 15 min. The solution was kept overnight, filtered washed, and dried for 12 h at 110 ^{o}C **[13]**.

c) Hybrid $CaSO_4$/PMMA nanocomposite (with ratio 1/10) was prepared by adding nano $CaSO_4$ solution (0.3 g) to PMMA solution (3 g) in 20 ml acetone. The mixture was stirred for 2 hs after which poured into a petri dish and dried at 110 ^{o}C for 12 h. The produced nanocomposite was milled and labeled as $CaSO_4$/PMMA.

d) Hybrid $TiSO_4$/PMMA nanocomposite (with ratio 1/10) was prepared by **(a)** stirring 24.8 g of PEG (M.W=200 g/mol) in a minimum amount of bidistilled water then added this solution to 4 g $TiSO_4$ solution dropwise, the mixture was maintained 4 h at room temperature. The mixture is filtered, washed, and dried at 110 ^{o}C for 12 h. **(b)** the nanocomposite $TiSO_4$/PMMA is prepared by the same previous method with adding the treated $TiSO_4$ instead of $CaSO_4$ to PMMA solution.

2.3. Catalyst characterization

The crystalline phase of nano $CaSO_4$ was investigated by XRD using a Pan Analytical Model X Pert Pro, which was equipped with CuK radiation (λ= 0.1542 nm), Ni-filter, and general area detector. The diffractograms were recorded in the 2θ range of 10–70◦ with a step size of 0.02 Å and a step time of 0.605 min. Nano $CaSO_4$ is also characterized by scanning electron microscopy (SEM) using a JEOL JSM-5300 instrument working at 30 kV. Microscopy images of nano $CaSO_4$ and nanocomposites ($CaSO_4$/PMMA and $TiSO_4$/PMMA) were obtained by transmission electron microscopy (TEM) using a JEOL JEM-1230. Thermo-gravimetric analysis (TGA) for the PMMA and its modified samples were executed using the instrument SDT Q600 V20.5 Build15. Fourier transform infrared spectroscopy for $CaSO_4$/PMMA has been executed to confirm its structure using the ATI Mattson genesis and FTIR spectrophotometer.

2.4. Screening experiment

The screening test was once performed to examine and the distinction between the efficiency of PMMA, $CaSO_4$/PMMA, and $TiSO_4$/PMMA in the Ca^{+2} and Mg^{+2} removal. The three one-of-a-kind treats had been utilized through the usage of a concentration of Ca^{+2} and Mg^{+2} 100 ppm, pH was once 6.8, and 0.6 g/L polymer dose for 120 minutes. The stirrer was used to shake the reaction mixture at room temperature. The concentration of Ca^{+2} and Mg^{+2} cations were determined experimentally according to ASTM D 4327 using Dionex IC model DX 600 equipped with high capacity columns using the following system: column, Ion Pac CS12A (4X 250 nm), eluent 20 mM Methane sulfonic acid, With injection volume 10 µl, 1.0 ml/min flow rate and Electrochemical detector (Dionex, ED 50) (Iftikhar, Yousaf, et al. 2020) and the removal efficiency was calculated using the following equation (Equation 1).

$$\text{Removal efficiency (\%)} = \frac{C_0 - C_e}{C_0} \text{ X } 100 \quad \text{(Eq. 1)}$$

Where C_0 and C_e are initial and equilibrium final concentrations (mg/L) of the Ca^{+2} and Mg^{+2} solutions.

2.5. Optimization process

The batch equilibration method used to be utilized to examine the sorption tendency of the synthesized chelating polymer to Ca^{+2} and Mg^{+2} cations **[14, 15]** and to determine the ideal adsorption conditions, such as the pH, contact time, temperature, preliminary attention of metallic ion, and the dose of the polymer samples. The sorption potential for Mg^{+2} and Ca^{+2}, under noncompetitive conditions, was once determined. The batch study used to look at the effect of contact time (15- 180 minutes), pH (2-14), adsorbent dose (0.2- 4 g/l), the awareness of cation solution (100-500 mg/l), and temperature (25- 60 ^oC) on check answer and stirred in a temperature-controlled shaker at a constant speed of 250 rpm. The effect of pH on Ca^{+2} and Mg^{+2} uptake was studied using HCl (0.1 M) and NaOH (0.1 M). Optimum conditions had been chosen for further studies. After equilibration, the residue concentration of metal ions used to be determined and the uptake efficiency percent calculated according to Eq. 1.

2.6. Modeling kinetics studies

The Kinetics of the adsorption manner was issued to the rate dedication of Ca^{+2} and Mg^{+2} removal using $CaSO_4$/PMMA and $TiSO_4$/PMMA that controlled the equilibrium time. The contact time between the adsorbent and the cationic metal ions is of sizeable importance in the treatment of wastewater with the aid of adsorption. The adsorption kinetics can be studied by adsorption based totally on the constant speed. This adsorption constant used to be an important aspect of the preference of material to be used for adsorption. For further investigation of the adsorption behavior, pseudo-first-order and pseudo-second-order kinetic models have been used to analyze the obtained data and can be summarized as follows.

The pseudo-first-order mode**l** was described by the following equation (Eq. 2):

$$\log (qe - qt) = \log qe - \frac{kft}{2.303} \quad \text{(Eq. 2)}$$

Where qe is adsorbed pollutants at equilibrium per unit weight of sorbent (mg g^{-1}), qt is adsorbed pollutants (mg g^{-1}), and k_1 is the rate constant per minute.

A plot of log (qe-qt) versus time (t) indicates a straight line of slope (k1/2.303) and an intercept of log (qe).

The pseudo-second-order model was analyzed by the following equation (Eq. 3):

$$\frac{t}{qt} = \frac{1}{k_2\, qe^2} + \frac{1}{qe} \quad \text{(Eq. 3)}$$

Where K_2 is the equilibrium rate constant (g mg^{-1} min^{-1}), qe and qt are the sorption capacities at equilibrium at a time (t).

A plot t/qt versus t shows a straight line of slope (1/qe) and an intercept of ($1/K_2q_e^2$).

2.7. Isotherm studies

The adsorption isotherm research was displayed to supply a basis for revealing adsorption behavior, indicating a feasible adsorption mechanism, and estimating adsorption capacity. To decide the mechanism of sorption of Ca^{+2} and Mg^{+2} through $TiSO_4$/PMMA and $CaSO_4$/PMMA respectively, the linear Langmuir and Freundlich isotherms were displayed:
Langmuir's sorption model was applied to determine the adsorption capacity of each material. It was expressed through the following equation (Equation 4):

$$\frac{Ce}{q_e} = \frac{Ce}{Q_{max}} + \frac{1}{bQ_{max}} \quad (Eq.\ 4)$$

Where q_e is the amount of metal ion sorbed (mg g^{-1}), *b* is a constant related to the adsorption/desorption capacity and Q_{max} is the maximum sorption capacity upon complete saturation of the surface.
Whereas, Freundlich isotherm "an empirical equation" was used to estimate the adsorption intensity of $TiSO_4$/PMMA towards Ca^{+2} and $CaSO_4$/PMMA towards Mg^{+2}. The following equation (Equation 5) was used to express the Freundlich isotherm:

$$\log q_e = \log k f + \frac{1}{n} \log C_e \quad (Eq.\ 5)$$

Where q_e, the adsorption density (mg of adsorbate adsorbed per each g of adsorbent). C_e is the concentration of pollutants in solution at equilibrium (mg L^{-1}), KF, and n are the Freundlich constants.

3. Results and discussion

3.1. Characterization of the prepared $CaSO_4$ and the nanocomposites

Figure 1 displays the XRD analysis of nano $CaSO_4$ indicating that the prepared sample is a crystalline phase of anhydrous calcium sulfate with the reference code No. (01-089-1458). The main diffraction peaks of $CaSO_4$ nanoparticles (as orthorhombic) are shown at 2 θ values of 14.78°, 25.72°, 29.77°, 31.97°, and 49.42°**[16]**. These positions of diffraction peaks were consistent with standard $CaSO_4$ powder diffraction data reported in the literature (JCPDS card No.-26-0392) for $CaSO_4$ nanoparticles **[16]**.

Figure 2 indicates the SEM and TEM of $CaSO_4$ respectively. The scanning electron microscope indicates that $CaSO_4$ has rectangular parallelepiped morphology **[17]**.

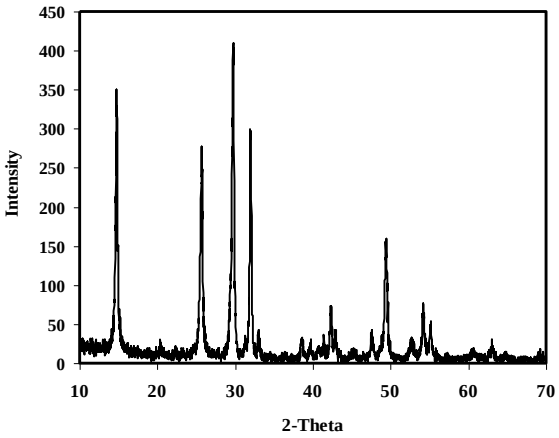

Figure 1. XRD of orthorhombic nano-$CaSO_4$ anhydrous.

The TEM indicates a hollow tabular crystal with a diameter ranged between 70 and 200 nm for the prepared $CaSO_4$ nanoparticles mostly due to the influence of PEG as a templating agent.

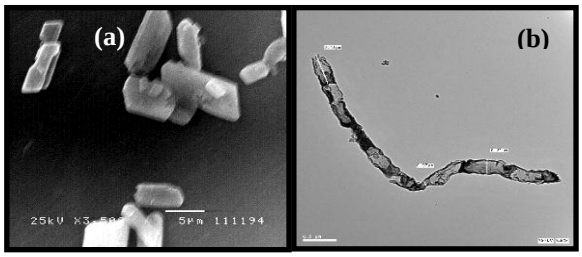

Figure 2. (a) SEM and, (b) TEM of $CaSO_4$.

Figure 3 shows the TEM micrographs of PMMA and its nanocomposites $CaSO_4$/PMMA, and $TiSO_4$/PMMA. Images of PMMA show a homogeneous surface of polymethyl methacrylate. On the other hand, the images of $CaSO_4$/PMMA show nanoparticles dispersed homogeneously through the PMMA matrix which indicating good dispersion and incorporation of $CaSO_4$ nanoparticles with the PMMA. The inset image shows the rectangular parallelepiped crystals of $CaSO_4$ that are dispersed with the polymer matrix. The image of $TiSO_4$/PMMA shows parallel layers of the nanocomposite matrix in which the titanium sulfate particles are well dispersed and interacted with the PMMA chains. Also, the titanium sulfate particles mostly play an important role in the morphology of the $TiSO_4$/PMMA matrix.

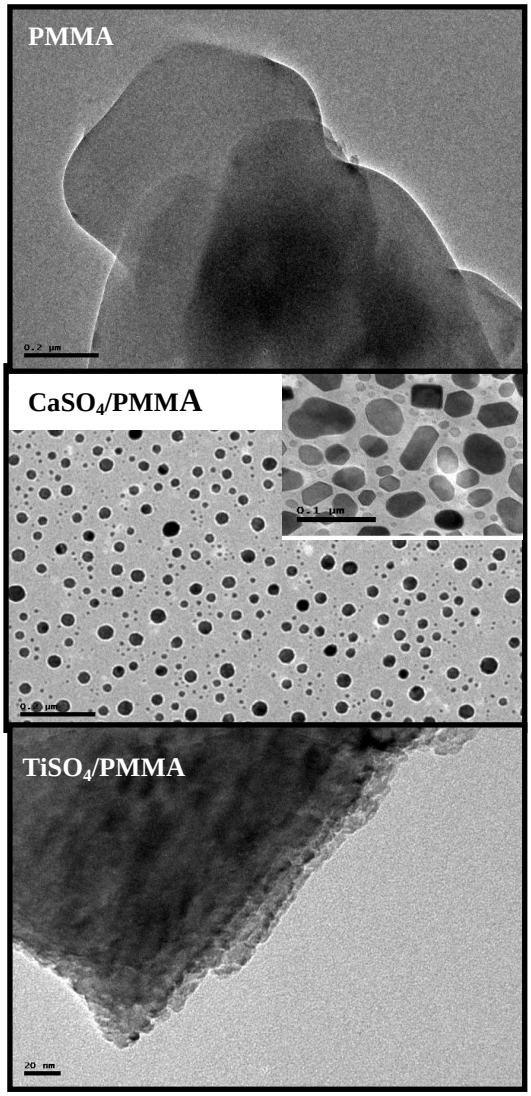

Figure 3. TEM of PMMA and its nanocomposites with $CaSO_4$ and $TISO_4$.

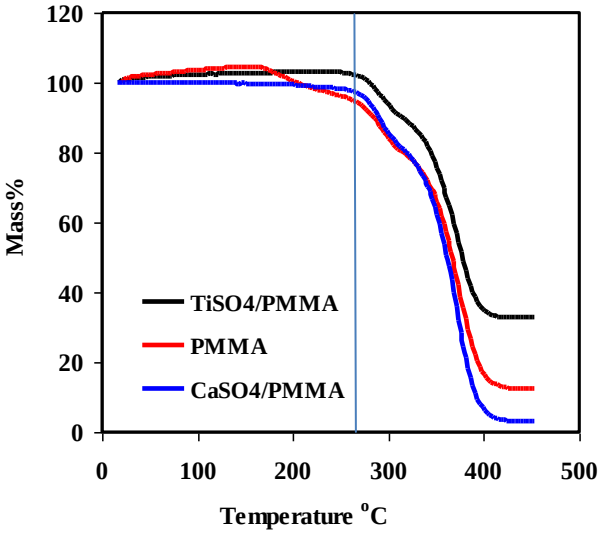

Figure 4. Effect of heating on the mass loss (TGA) of PMMA, $TiSO_4$/PMMA, and $CaSO_4$/PMMA.

Figure 4 shows the thermo-gravimetric analysis (TGA) of PMMA, $CaSO_4$/PMMA, and $TiSO_4$/PMMA samples. The figure indicates the Mass% loss due to heating from the room temperature to ~ 450 ^oC. The thermal stability of PMMA without modification is extended up to ~ 170 ^oC then start losing weight. On the other hand, modified nanocomposites $CaSO_4$/PMMA, and $TiSO_4$/PMMA are stable up to ~ 270 ^oC indicating more thermal stability. This confirms that $CaSO_4$ and $TiSO_4$ are strongly incorporated and bonded with PMMA functional groups. Also, the structures of the three samples are not affected by heating during the water treatment process.

3.2.The postulated structure of nanocomposites

According to previous publications **[10, 11]** and the TEM in the present study, the structure of $CaSO_4$/PMMA and $TiSO_4$/PMMA can be postulated. TEM indicates that the orthorhombic $CaSO_4$ crystals are homogeneously spread in the PMMA matrix as shown in the TEM (**Figure 3)**. Mostly, there is an interlinkage between the ester group of PMMA and Ca of $CaSO_4$/PMMA hybrid (represented in **Figure 5a**). Also, Ti of titanium sulfate interacted with the ester group of the polymer matrix. The terminal olefinic groups of polymer chains especially interacted with the sulfate anions. The morphology of $TiSO_4$/PMMA nanocomposite is different indicating that $TiSO_4$ bridged between the polymer chains. So, $TiSO_4$/PMMA nanocomposite has parallel plate morphology as shown in its TEM (**Figure 3**), accordingly has been postulated in **Figure 5b.** These interactions may be a chemical reaction, physical interaction, or intradiffusion process.

Figure 6 displays the FTIR spectroscopic analysis of $CaSO_4$/PMMA nanocomposite to confirm its structure as an example of hybrid PMMA. According to a previous publication, the characteristic bands of $CaSO_4$ appear at 3617.07, 3554.29, 1621.04, 658.05, 598.03, and 482.35 cm^{-1}**[18]**. The band appeared at 3440.11 cm^{-1} probably due to the CH_2 stretch attached to SO_4^{-2} as shown in the postulated structure. The characteristic band of the –C=O stretch of the ester group appears at 1747.68 cm^{-1}. This group should appear between 1711-1728 cm^{-1} according to a previous publication **[19]**. The shift to a larger wavenumber is due to its interaction with electron-

withdrawing groups, here mostly it is the Ca^{+2} of $CaSO_4$ (see **Fig. 5a**).

$CaSO_4$/PMMA nanocomposites toward the uptake of Ca^{+2} and Mg^{+2} respectively mostly due to the ionic

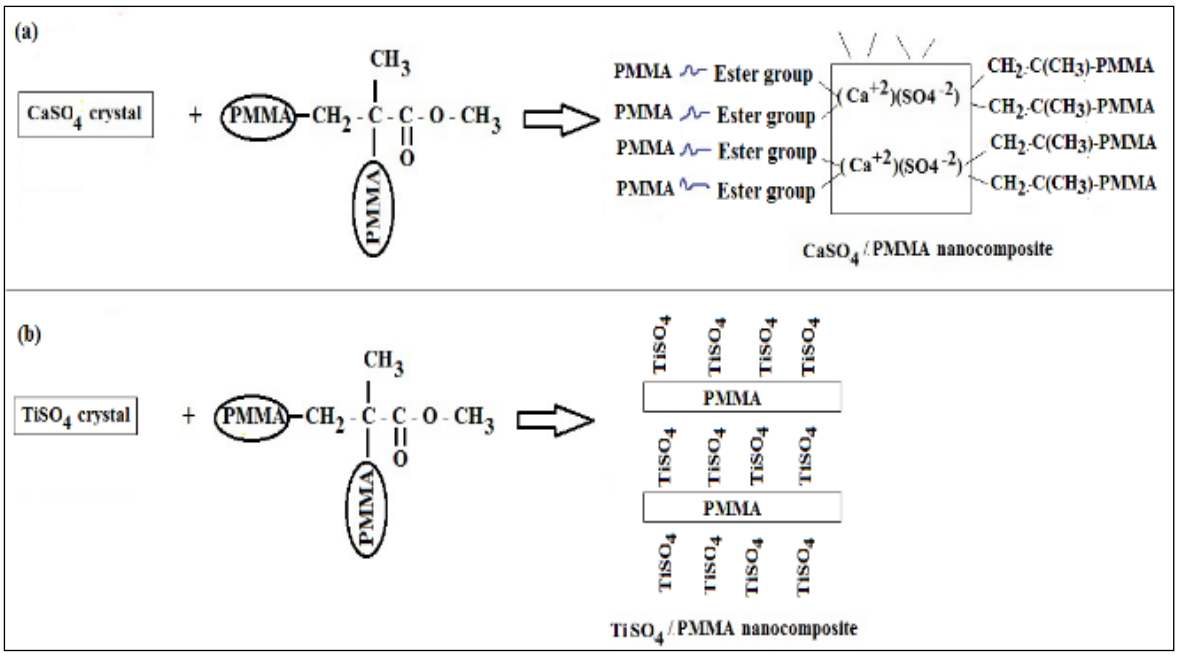

Figure 5. The postulated structure of (a) $CaSO_4$/PMMA and (b) $TiSO_4$/PMMA nanocomposites.

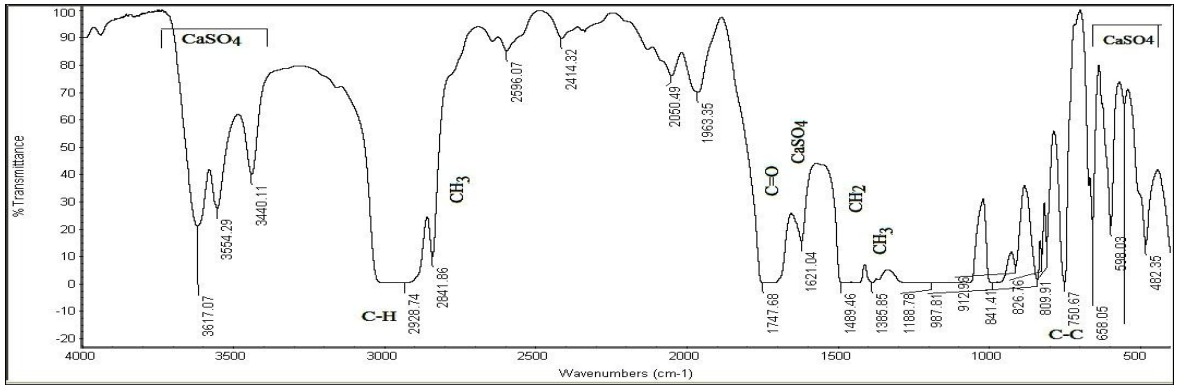

Figure 6. FTIR of $CaSO_4$/PMMA nanocomposite.

3.3. Screening process

The experiments were established using PMMA with/without modification to screen the best samples that can be included in the next experiments and achieve high Ca^{+2} and Mg^{+2} removal efficiency. The experiment proceeded using 100 ppm of Ca^{+2} or Mg^{+2}, 0.6 g/l catalyst dose, pH 6.8 at room temperature after 120 min with stirring. It has been found that the high efficiency of Ca^{+2} removal (is 42.64%) has been done with a $TiSO_4$/PMMA, while the high efficiency of Mg^{+2} removal (29.76%) has been done by $CaSO_4$/PMMA see **Figure 7**. The observed selectivity of $TiSO_4$/PMMA and radii of Ca^{+2} (114pm) and Mg^{+2} (86 pm). The TEM images of catalysts indicate the wider porosity of $TiSO_4$/PMMA relative to $CaSO_4$/PMMA and PMMA respectively. Also, the removal ability of PMMA without modification for Ca^{+2} was 8.9% and Mg^{+2} was 10%. It can be deduced that the morphology of the polymer samples is critical for the cation removal process.

3.4. Optimization process results

According to the screening experiments, the adsorption selectivity of $TiSO_4$/PMMA and

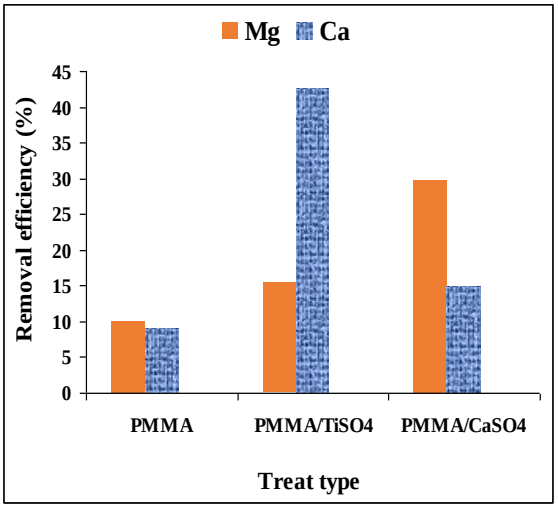

Figure 7. Screening experiments for Ca^{+2} and Mg^{+2} removal using PMMA, PMMA/$TiSO_4$, and PMMA/$CaSO_4$.

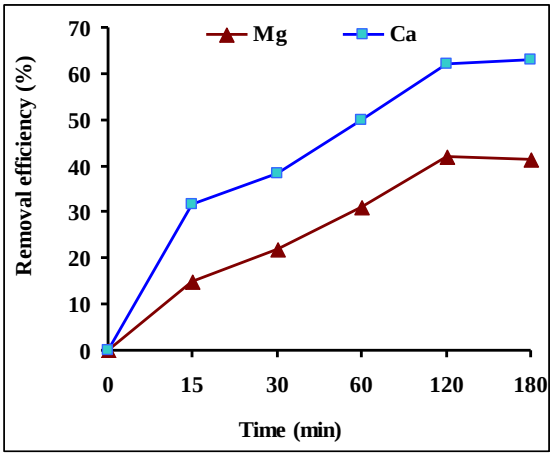

Figure 8. The influence of contact time on the adsorption of Mg^{+2} by $CaSO_4$/PMMA and Ca^{+2} by $TiSO_4$/PMMA nanocomposite catalysts.

$CaSO_4$/PMMA is toward Ca^{+2} and Mg^{+2} respectively. Accordingly, the optimization conditions have been studied for the uptaking efficiency of $TiSO_4$/PMMA for Ca^{+2} and $CaSO_4$/PMMA for Mg^{+2}.

3.4.1. Effect of contact time

Figure 8 indicates the adsorption of Mg^{+2} on $CaSO_4$/PMMA and Ca^{+2} on $TiSO_4$/PMMA from the solution as a result of contact time and the other variables are pH 6.8, 100 mg/l cation solution concentration, 1 g/l catalyst dose at room temperature with constant stirring. It can be noted from the figure that the adsorption of both pollutants increased as contact time increased. The most adsorption of Ca^{+2} was 63% at 180 min and Mg^{+2} was 42% at 120 min. Huanxin et al., (2012) cited that similarly increase in contact time had no good-sized effect on modified PMMA adsorption capacity, confirms that Ca^{+2} and Mg^{+2} cations at the beginning diffuse and interact rapidly with the available ester groups of PMMA chains, suggesting the formation of metal–carboxylate complex through unidentate chelating coordination. Also, $TiSO_4$ and $CaSO_4$ frequently acted as a spacer arm that ought to catch divalent cations without problems **[10, 20]**. This was confirmed by the TEM analysis and the postulated structure of the hybrid materials. The typical interior structure of $TiSO_4$/PMMA shows the lamellar structure **(Figures 3, 5).**

The distinct boundary between $TiSO_4$ and PMMA gives good chance to the intradiffusion of Ca^{+2} (its ionic radius is 114 pm) between the porous $TiSO_4$/PMMA layers and interaction with O-CH_3 groups. Also, the smaller Mg^{+2} (86 pm) has a suitable chance to diffuse between PMMA chains and interact with the available O-CH_3 functional groups in $CaSO_4$/PMMA

3.4.2. Effect of pH

It was reported that the pH value strongly influenced the adsorption of cationic metallic ions by the suitable sorbents, as it determines the adsorbent surface charge, the degree of solute ionization, and the specificity of the adsorbate **[21]**. The influence of pH on the uptaking of Ca^{+2} and Mg^{+2} cations used to be examined in the 2–14 range and the other variables are 120 min contact time, 100 mg/l cation concentration, 1 g/l catalytic dose at room temperature with stirring constantly.

Figure 9 confirms that the complexation manner of cationic metal ions is sensitive to pH changes. The elimination efficiency of Ca^{+2} and Mg^{+2} cations at decrease pH regions was inhibited but increased by increasing pH value. Previous publications indicated that the uptaking of Ca^{+2} and Mg^{+2} cations is affected by the structural properties of the adsorbent (e.g., purposeful groups, porosity, surface area, and swelling degree), the chelate-formation rate between the complexing ligand and the metal ions, and many different factors. Therefore, the optimum pH may also be in acidic, neutral, or alkaline regions **[4, 22, 23]**.

According to **Figure 9**, the results indicated that in our work the removal efficiency of metal cations increased by increasing pH up to 8 then decreased and increased with pH. The highest removal percent of Ca^{+2} and Mg^{+2} are nearly 67% and 65% respectively.

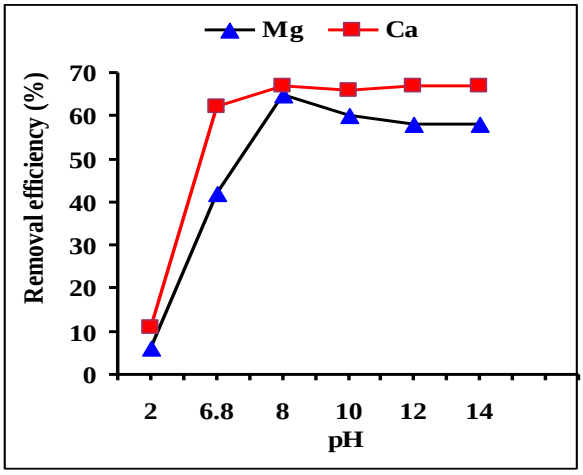

Figure 9. The influence of pH on adsorption of Mg^{+2} by $CaSO_4$/PMMA and Ca^{+2} by $TiSO_4$/PMMA nanocomposite catalysts.

The uptaking efficiency of Ca^{+2} is high relative to Mg^{+2}. The basic solution enriched with OH^- mostly enhances the hydrolysis of -O-CH_3 group producing carboxylate group -COO^- and CH_3OH, then cations interact easily with the carboxylate group enhancing its removal according to **Equation 6 [24, 25]**. On the other hand, in an acidic solution enriched with H^+, the ester group hydrolyzed to carboxylic group (-COOH) and methanol molecule according to **Equation 7**. So, a competition effect between H^+ and cationic metal ions inhibits the uptake of cations in acidic solutions. If the composite is prepared from polymethacrylic acid, a moderate alkaline solution may enhance the removal of cations without producing methanol as a byproduct, according to the postulated **Equation 8** and this idea can be studied in the future.

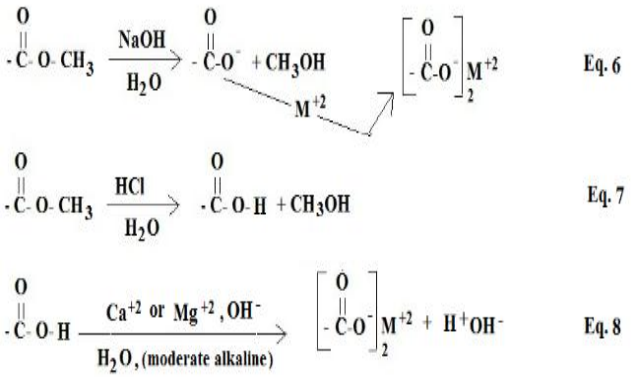

3.4.3. Effect of dose

The batch study was set up to determine the effect of the $CaSO_4$/PMMA and $TiSO_4$/PMMA dose (from 0.2 g/l up to 4 g/l) on Mg^{+2} and Ca^{+2} adsorption respectively, other factors are pH 8, 120 min contact, 100 mg/l cations concentration, at room temperature with constant stirring and the results are shown in **Figure 10**. The results indicate that the removal percent of Ca^{+2} and Mg^{+2} was increased by increasing the adsorbent dosage until it got its highest value of 67% for Ca^{+2} and 65% for Mg^{+2} using 1 g/l. After which, the more the dose of the adsorbent used, the lesser the number of metal ions adsorbed. It can be summarized that the number of fixation sites of the metal Ca^{+2} or Mg^{+2} ions is mostly reduced, which could be interpreted by the presence of the electrostatic interactions between binding sites itself and/or ester groups hydrolyzed together, so the metal ions uptaking will be blocked **[26]**.

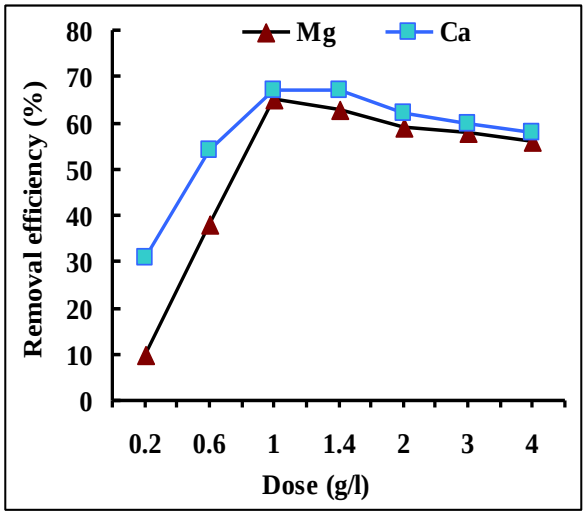

Figure 10. Effect of nanocomposite dose on adsorption of Ca^{+2} and Mg^{+2} onto $TiSO_4$/PMMA, and $CaSO_4$/PMMA, respectively

3.4.4. Effect of initial concentration

In the current work, the influences of Ca^{+2} and Mg^{+2} initial concentration on the adsorption were investigated at room temperature and certain pH value 8 using 1g/l of $CaSO_4$/PMMA and $TiSO_4$/PMMA, 120 min contact with constant stirring. The effect of different Ca^{+2} and Mg^{+2} concentrations; 100, 300, 500 mg/l were studied. According to **Figure 11**, the maximum removal % of Ca^{+2} and Mg^{+2} ions is 67% and 65% at 100 mg/l ions concentration. As the cation concentration increase, the removal% decrease. This is because at a lower

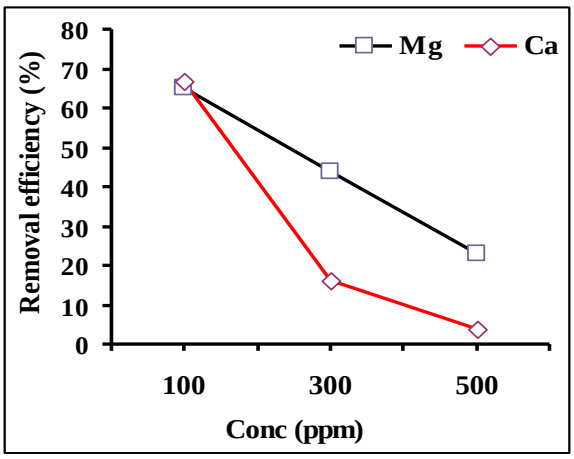

Figure 11. The influence of different initial concentrations of Mg^{+2} by $CaSO_4$/PMMA and Ca^{+2} by $TiSO_4$/PMMA.

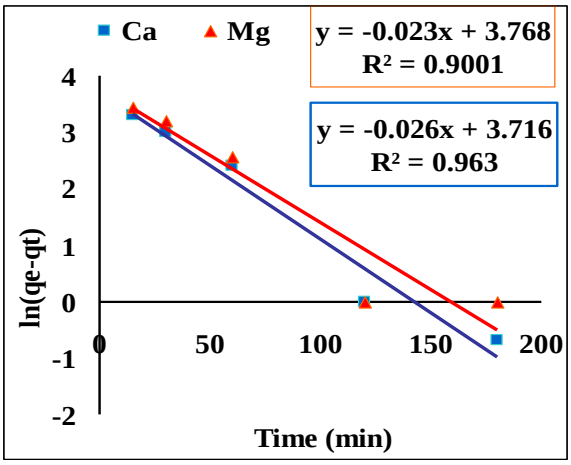

Figure 12. Pseudo 1st order kinetics for adsorption of Ca^{+2} and Mg^{+2} onto $TiSO_4$/PMMA, and $CaSO_4$/PMMA, respectively.

concentration more polymer pore spaces were available for Ca^{+2} or Mg^{+2} which are mostly saturated with 100 mg/l. Above this concentration, the adsorption capacity of the polymer diminished considerably due to the reduced availability of free pore spaces.

3.5. Modeling kinetics studies

Figures (12, 13) showed the pseudo-first-order and Pseudo second-order studies for the cationic metal ions removal process by using modified PMMA and the calculated constants and correlation coefficients were shown in **Table 1**. It was observed that the pseudo-second-order kinetic model adequately fit the experimental values (R^2 0.98 for adsorption of Mg^{+2}) onto $CaSO_4$/PMMA which confirms diffusion is the main adsorption model for adsorption processes. In contrast, the pseudo-second-order rate equation adequately fit the experimental values (R^2 0.99 for adsorption of Ca^{+2}) onto $TiSO_4$/PMMA agreed well with the experimental data.
The pseudo-second-order model well represented the kinetic data based on the excellent goodness of the fit (R^2) as well as the agreement of the equilibrium adsorption capacity predicted by the model (qe) with the experimental ones.

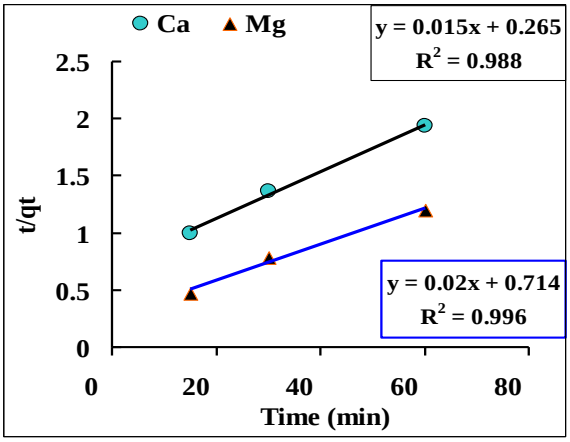

Figure 13. Pseudo 2nd order kinetics for adsorption of Ca^{+2} and Mg^{+2} onto $TiSO_4$/PMMA, and $CaSO_4$/PMMA, respectively.

Table (1) kinetic parameters of Mg^{2+} and Ca^{2+}

Metal cations	Adsorbent	$q_{e,exp}$ (mg/g)	Pseudo-first-order kinetics model			Pseudo-second-order kinetics model		
			q_e (mg/g)	k_1 (min^{-1})	R^2	q_e (mg/g)	k_2 (mg/(g min))	R^2
Mg(II)	$CaSO_4$/PMMA	63	5205.75	0.0548	0.9	63.29	0.00094	0.98
Ca(II)	$TiSO_4$/PMMA	42	5866.78	0.0601	0.96	48.78	0.00059	0.99

3.6. Adsorption Isotherm studies

Langmuir and Freundlich isotherm linear plots were represented in **Figures 14, 15** and the calculated constant and correlation co-efficient R^2 were shown in **Table 2**. According to the Langmuir isotherm model, the calculated R^2 values for Ca^{+2} and Mg^{+2} adsorption were found to be 0.897 and 0.917 and according to the Freundlich model, R^2 values were found to be 0.016 and 0.79 for Ca^{+2} and Mg^{+2}, respectively. The obtained highest R^2 values for the Langmuir isotherm model revealed that cationic metal ions adsorption onto $CaSO_4$/PMMA and $TiSO_4$/PMMA followed the Langmuir isotherm model. The best fitting of the Langmuir model indicated the homogeneous and monolayer adsorption of Ca^{+2} and Mg^{+2} onto $TiSO_4$/PMMA and $CaSO_4$/PMMA respectively. The Langmuir monolayer capacity values (mg/g) have been estimated to be 85.47 mg/g and 344.82 mg/g for Ca^{+2} and Mg^{+2}, respectively (Table 2). High-capacity values suggest the prospective use of modified PMMA as an adsorbent for the treatment of Ca^{+2} and Mg^{+2} cations and indicated physisorption of cationic metal ions on the adsorbent. Comparing the removal% of Ca^{+2} or Mg^{+2} with the capacity values of their adsorbents $TiSO_4$/PMMA and $CaSO_4$/PMMA respectively indicate that Ca^{+2} cations may have the capability to be adsorbed as multilayer so, its removal% is high relative to Mg cations.

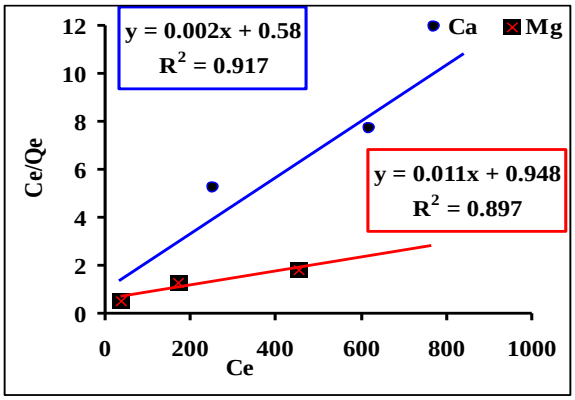

Figure 14. Adsorption Langmuir isotherm for adsorption of Ca^{+2} and Mg^{+2} onto $TiSO_4$/PMMA, and $CaSO_4$/PMMA, respectively

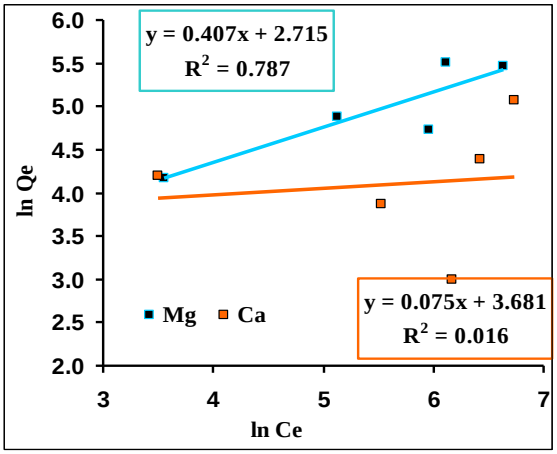

Figure 15. Adsorption Freundlich isotherm for adsorption of Ca^{+2} and Mg^{+2} onto $TiSO_4$/PMMA, and $CaSO_4$/PMMA, respectively.

3.7. Adsorption thermodynamics

Figure 16 presents the plot of percentage adsorption of Ca^{+2} and Mg^{+2} by modified PMMA samples at varying temperatures with reached optimum sorption of 65% for Mg^{+2} occurring at 25 °C while 87.5% for Ca^{+2} occurring at 40°C. The plot showed that an additional temperature rise resulted in a minor decrease in adsorption. This is in harmony with the general principle that physical adsorption declines with an increase in temperature, i.e. molecules adsorbed earlier on a surface tend to desorb from it at elevated temperatures **[27]**. This behavior may result from the increased kinetic energy of metal ions that

Table (2) Adsorption isotherm parameters of Mg2+ and Ca2+

Metal ions	Adsorbent	Langmuir equation model			Freundlich equation model		
		q_m (mg/g)	b	R^2	k_F	1/n	R^2
Mg(II)	$CaSO_4$/PMMA	344.82	0.01233	0.897	1.50160227	0.4079	0.79
Ca(II)	$TiSO_4$/PMMA	85.07	0.00499	0.917	0.2036925	0.075	0.016

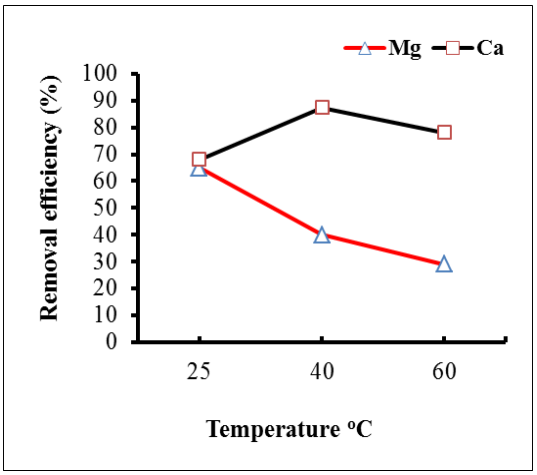

Figure 16. Effect of temperature on ions uptake efficiency of Ca^{+2} and Mg^{+2} onto $TiSO_4$/PMMA, and $CaSO_4$/PMMA, respectively.

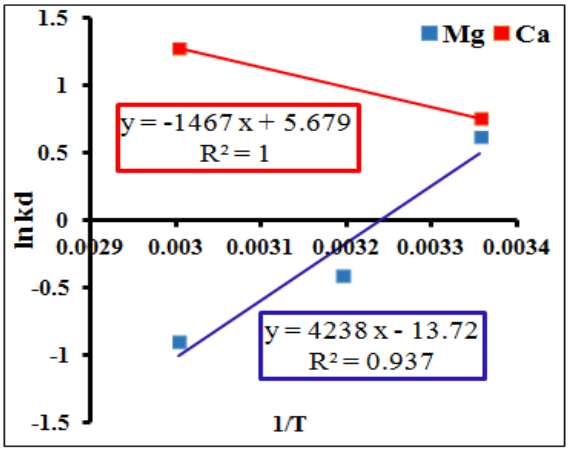

Figure 17. Adsorption thermodynamics, Van't Hoff plot of $\ln K_d$ versus 1/T of ions uptake efficiency onto modified PMMA.

resulted in the decrease in attraction forces between the polymer and metal ions, and a decrease in the rigidity of the polymer's boundary layers resulted in a higher propensity of Ca^{+2} and Mg^{+2} cations to escape the polymer.

Low temperatures enable the adsorption by modified PMMA polymer of Ca^{+2} and Mg^{+2} cations, this suggested a diffusion-controlled kinetic process. The sorption process was not improved by the high temperatures.

Figure 17 shows the effect of temperature on the distribution coefficient and the values of enthalpy (ΔH^o) and entropy (ΔS^o) were calculated from the slope and intercept of the plot of ln Kd vs. 1/T by using the next equations:

$$\triangle G^o = - RT \ln K_d \qquad (Eq.\ 9)$$

$$\ln K_d = \frac{\triangle S^o}{R} - \frac{H^o}{R} T \qquad (Eq.\ 10)$$

Where *K*d is the distribution coefficient, ΔS^o, ΔH^o and ΔG^o are the changes of entropy, enthalpy, and the Gibbs free energy, *T* is the temperature (K), *R* is the gas constant (8.3145 J mol−1 K−1). The thermodynamic data calculated by **Equations 9 and 10**.

The thermodynamic parameters for adsorption systems are scheduled in **Table 3**. Because the standard enthalpy changes $\Delta H°$ for the adsorption $^+$ process is positive (10.88 KJ/mol), the adsorption process of Ca^{+2} by the adsorbent $TiSO_4$/PMMA is endothermic proposing that the adsorption proceeds via chemisorption. A positive value between (1.86 to 5.8 KJ/mol) was obtained for ΔG^o confirms the spontaneous nature of Ca^{+2} adsorption process. The positive value of $\Delta S°$ (0.0455 KJ/mol) indicates raised randomness in the solid/interface during the adsorption of Ca^{+2} ions. Positive entropy values indicate that Ca^{+2} on $TiSO_4$/PMMA breaks the hydration armor before adsorption **[28]**. Whereas for Mg^{+2} ions the ΔH^o values are negative (-35.24 KJ/mol), demonstrating the exothermic nature of these adsorptions, which is compatible with the experimental observations. A negative value of entropy change ΔS^o (-0.11 KJ/mol) also displays a decreased disorder at the solid/liquid interface during the adsorption process causing the adsorbate ions/polymer to escape from the solid phase to the liquid phase. Therefore, the amount of adsorbate that can be adsorbed will decrease but the ΔG^o was

Table (3) Thermodynamic parameters of Mg^{2+} and Ca^2

Metal cations	Adsorbent	Thermodynamic parameters				
		ΔG^0 (kJ mol^{-1})			ΔH^0 (kJ mol^{-1})	ΔS^0 (J mol^{-1} K^{-1})
		298 k	313 k	343 k		
Mg(II)	$CaSO_4$/PMMA	1.5	-1.05	-2.47	-35.24	-0.11
Ca(II)	$TiSO_4$/PMMA	1.86	3.3	5.8	10.88	0.045

positive (1.5 KJ/mol) when the adsorption temperature at 25°C, so the adsorption process of Mg^{+2} onto $CaSO_4$/PMMA was spontaneous while negative value at 40°C and 60°C show a non-spontaneous process.

4. Conclusions

Herein, $TiSO_4$/PMMA and $CaSO_4$/PMMA nanocomposites have been successfully synthesized, characterized, and applied for removal of Ca^{+2} and Mg^{+2} respectively. The prepared nano $CaSO_4$ has rectangular parallelepiped morphology which is dispersed homogeneously with the polymer matrix in $CaSO_4$/PMMA. FTIR confirms the presence and interaction of $CaSO_4$ with the carbonyl ester group and CH_2 of PMMA chains. Also, $TiSO_4$ interacted with PMMA resulting in parallel layers morphology in $TiSO_4$/PMMA. The structures of the synthesized hybrid PMMA composites are postulated. Incorporating the inorganic salts with the polymer increased the thermal stability of the produced hybrids. Batch adsorption experiments demonstrated that the contact time, initial concentration, adsorbent dosage, and solution pH have significant effects on pollutant adsorption. The maximum removal percent was 65% for Mg^{+2} by $CaSO_4$/PMMA at 25 °C and was 87.5% for Ca^{+2} by $TiSO_4$/PMMA at 40°C using 1g/l dose, pH 8 at 120 min. Kinetics studies have revealed that the pseudo-second-order kinetic model. The thermodynamic parameters suggested that the Ca^{+2} adsorption onto $TiSO_4$/PMMA was a spontaneous process while for Mg^{+2} adsorption onto $CaSO_4$/PMMA was a spontaneous process at 25°C and non-spontaneous at 40°C and 60°C. The adsorption isotherms fitted well with the Langmuir isotherm equilibrium model. Based on this study, it can be concluded that $TiSO_4$/PMMA and $CaSO_4$/PMMA were efficient adsorbents for the removal of cationic metal ions from the aqueous solution. Equations 6, and 7 indicated that methanol is a byproduct in acidic and alkaline solutions, equation 9 indicated that polymethacrylic acid does not produce the methanol in moderate and alkaline solutions. So in the future, we can prepare the hybrid nanocomposites of methacrylic acid (to avoid the formation of the toxic methanol) and test their efficiency in the removal of metal cations.

5. Conflicts of interest

There is no conflict of interest.

6. References

1. Malana M.A. and Khosa M.A., Groundwater pollution with special focus on arsenic, Dera Ghazi Khan-Pakistan.*Journal of Saudi Chemical Society*, **15**(1), 39-47(2011).
2. Narany T.S., Sefie A., and Aris A. Z., The long-term impacts of anthropogenic and natural processes on groundwater deterioration in a multilayered aquifer.*Science of the total environment*, **630**, 931-942(2018).
3. Liu W., Singh R. P., Jothivel S., and Fu D., Evaluation of groundwater hardness removal using activated clinoptilolite.*Environmental Science and Pollution Research*, 1-9(2019).
4. Sepehr M. N., Zarrabi M., Kazemian H., Amrane A., Yaghmaian K., and Ghaffari H. R., Removal of hardness agents, calcium and magnesium, by natural and alkaline modified pumice stones in single and binary systems.*Applied Surface Science*,**274**, 295-305(2013).
5. Gholamhossein M. G., Moshiri P., Dinari M., and Steiniger F., In situ synthesis of nanocomposite materials based on modified-mesoporous silica MCM-41 and methyl methacrylate for copper (II) adsorption from aqueous solution.*Journal of the Iranian Chemical Society*, **16**(7) 1491-1500(2019).
6. Yadav V.B., Gadi R., and Kalra S., Clay based nanocomposites for removal of heavy metals from water: a review.*Journal of environmental management*, **232**, 803-817(2019).
7. Kenawy I. M. M., Eldefrawy M. M., Eltabey R. M. and ZAKI E. G., Melamine grafted chitosan-montmorillonite nanocomposite for ferric ions adsorption: Central composite design optimization study.*Journal of Cleaner Production*, **241**, 118189(2019).
8. Phakatkar A. H., Shirdar M. R. , Qi ML, Taheri M. M., Narayanan S., Foroozan T., Sharifi-Asl S., Huang Z., Agrawal M., Lu YP., Shahbazian-Yassar R., and Shokuhfar T., Novel PMMA bone cement nanocomposites containing magnesium phosphate nanosheets and hydroxyapatite nanofibers.*Materials Science and Engineering:C*, **109**, 110497(2020).
9. Pal, M.K., B. Singh, and J. Gautam, Thermal and Electrical behaviour of CaSO4 nanoparticles mixed with Polymethylmethacylate and Polystyrene Polymer matrix.*Archives of Applied Science Research*, **1**(2), 313-319(2009)..
10. Ju H., Feng X., Ye Y., Zhang L., Pan H., Campbell C. T., and Zhu J., Ca carboxylate formation at the calcium/poly (methyl methacrylate) interface.*The Journal of Physical Chemistry C*, **116**(38), 20465-20471(2012).
11. Zhu J., Goetsch P., Ruzycki N., and Campbell C. T., Adsorption energy, growth mode, and sticking probability of Ca on poly (methyl methacrylate) surfaces with and without electron

damage.*Journal of the American Chemical Society*,**129**(20), 6432-6441(2007).
12. Solyman S., M., Azzam E., and Sayyah *S.*, The performance of modified nanoclay using polymeric thiol surfactants assembled on gold nanoparticles in heterogeneous bulk polymerization of methyl methacrylate.*Applied Catalysis A: General*, **475**, 218-225(2014).
13. Ghanshyam B., Sonawane S. S., Wasewar K. L., Rathod A. P., Shirish H. S., and Navin G. S., Synthesis of CaSO4 nanoparticles and its effect on PA6/CaSO4 nanocomposite for investigation of thermal and viscoelastic properties.*Research Journal of Chemistry and Environment*, 21(11), 39-44(2017).
14. Chandra D., Das S.K., and Bhaumik A., A fluorophore grafted 2D-hexagonal mesoporous organosilica: Excellent ion-exchanger for the removal of heavy metal ions from wastewater. *Microporous and mesoporous materials*, **128**(1-3). 34-40(2010.).
15. Younes A.A., El-Maghrabi H.H. and Ali H.R., *Novel polyacrylamide-based solid scale inhibitor.* Journal of hazardous materials, **334**, p. 1-9(2017).
16. Pal M.K., and Gautam J., *Effects of inorganic nanofillers on the thermal degradation and UV-absorbance properties of polyvinyl acetate.* Journal of thermal analysis and calorimetry, **111**(1), p. 689-701(2013.).
17. Shinsho K., Harada K., Yamamoto Y., and Urushiyama A., *Differences in glow curves structure of nano-and microcrystals of CaSO4: Dy measured at a low heating rate.* Radiation measurements, **43**(2-6), p. 236-240(2008).
18. Osterwalder N., Loher S., Grass R. N., Brunner T. J., Limbach L. K., Halim S. C., and Stark W. J., *Preparation of nano-gypsum from anhydrite nanoparticles: Strongly increased Vickers hardness and formation of calcium sulfate nano-needles.* Journal of Nanoparticle Research, **9**(2), p. 275-281(2007).
19. Rai V., Mukherjee C., and Jain B., *Optical properties (uv-vis and ftir) of gamma irradiated polymethyl methacrylate (pmma).* arXiv preprint arXiv:1611.02129(2016). https://arxiv.org/ftp/arxiv/papers/1611/1611.02129.pdf
20. Kurniawan A., Kosasih, A. N., Febrianto J., Ju Yi-H., Sunarso J., Indraswati N.,and Ismadji S., *Evaluation of cassava peel waste as low cost biosorbent for Ni-sorption: Equilibrium, kinetics, thermodynamics and mechanism.* Chemical engineering journal, **172**(1), p. 158-166(2011).
21. Amuda O., Giwa A., and Bello I., *Removal of heavy metal from industrial wastewater using modified activated coconut shell carbon.* Biochemical Engineering Journal, **36**(2), p. 174-181(2007).
22. Cetin G., *Removal of hardness of earth alkaline metals from aqueous solutions by ion exchange method.* ISRN Analytical Chemistry, 2014, Article ID 621794, 7 pages (2014). http://dx.doi.org/10.1155/2014/621794.
23. Denizli A., Denizli A., Buyuktuncel S.E., Tuncel A., Bektas S., and Genç Ö., *Batch removal of lead ions from aquatic solutions by polyethyleneglycol-methacrylate gel beads carrying cibacron blue F3GA.* Environmental Technology, **21**(6) p. 609-614(2000).
24. Smets G. and Loecker W. De., *Alkaline hydrolysis of methacrylic acid–ester copolymers.* Journal of Polymer Science, **41**(138), p. 375-380(1959).
25. Ayre W.N., Denyer S.P. and Evans S.L. *Ageing and moisture uptake in polymethyl methacrylate (PMMA) bone cements.* journal of the mechanical behavior of biomedical materials, **32**, p. 76-88(2014).
26. Kundu D., Hazra C., Chatterjee A., Chaudhari A., and Mishra S., *Retraction: Sonochemical synthesis of poly (methyl methacrylate) core–surfactin shell nanoparticles for recyclable removal of heavy metal ions and its cytotoxicity.* RSC Advances, **4**(95): p. 52949-52949(2014).
27. Abasi C., Donbebe W., and Dikio E. K., *Adsorption Study of Lead (II) Ions on Poly (methyl methacrylate) Waste Material.* Asian Journal of Chemistry, **30**(4): p. 859-867(2018).
28. Huang W., Chen J., He F., Tang J., Li D., Zhu Y., and Zhang Y., *Effective phosphate adsorption by Zr/Al-pillared montmorillonite: insight into equilibrium, kinetics, and thermodynamics.* Applied Clay Science, **104**: p. 252-260(2015).